Semiconductor-metal nanoparticle molecules in a magnetic field: Spin-plasmon and exciton-plasmon interactions

Alexander O. Govorov*
Department of Physics and Astronomy, Ohio University, Athens, Ohio 45701, USA
(Received 15 July 2010; revised manuscript received 19 September 2010; published 25 October 2010)

Excitons and plasmons in hybrid semiconductor-metal nanostructures strongly interact via the Coulomb forces. Simultaneously, excitons in semiconductors experience typically strong intrinsic spin-dependent interactions that result in efficient coupling between spins of excitons and dynamic electric fields of photons. A joint action of the exciton-plasmon and spin-dependent interactions leads to a coupling between spins and plasmons. Calculated optical spectra of hybrid nanoparticle molecules reveal such spin-plasmon coupling. The spin-plasmon coupling creates spin-dependent Lamb shifts of excitons. In the presence of the exciton-plasmon interaction, the spin splitting in the exciton spectrum can decrease or even vanish under certain conditions. In a magnetic field, the spin-plasmon interaction strongly alters optical spin-dependent selection rules, leading to forbidden optical lines. Allowed and forbidden optical transitions in the presence of the exciton-plasmon and spin-plasmon interactions typically acquire Fano-type or antiresonance shapes. Plasmon-induced interactions in semiconductor-metal nanocrystal structures suggest interesting opportunities for tailoring of spin and optical spectra of excitons.

DOI: 10.1103/PhysRevB.82.155322 PACS number(s): 78.67.Hc, 78.40.Fy, 78.67.Bf

I. INTRODUCTION

Photons and electron spins in semiconductors strongly couple due to the spin-orbit interaction in the valence band, enabling the effect of optical spin orientation of carriers.[1,2] In semiconductor quantum dots (SQDs), spin-dependent interactions in excitons often govern the fine structure of excitonic spectra.[3–10] Another important class of interactions in solid-state and molecular nanostructures comes from the Coulomb coupling between excitons and plasmons. The interaction between optical dipoles (excitons) and plasmons may have Coulomb and electromagnetic components and can be coherent or incoherent.[11–21] Exciton-plasmon and electron-plasmon interactions are observed and studied in many material systems, including solid-state nanoelectronics devices,[22–24] colloidal nanoassemblies,[11,20,25–30] molecular-metal systems,[11,21,31,32] etc. A recent paper[33] reported the effects of strong coupling between optically excited spin-polarized carriers and plasmons in core-shell colloidal nanocrystals.

Here we propose and study theoretically hybrid systems where spin-polarized excitons and plasmons become strongly coupled. These systems comprise self-assembled SQDs and metal nanoparticles (MNPs). The coupling between spin-polarized excitons and plasmons occur via the dynamic Coulomb interaction. The Coulomb interaction itself does not depend on the spin coordinates. However, the Coulomb interaction can create spin-flip transitions and can involve spins if an exciton Hamiltonian has spin-dependent terms and the resulting exciton wave functions involve the spin coordinates in a nontrivial way.[34,35] Indeed, the exciton Hamiltonian of SQD incorporates the spin-orbit interaction in the valence band and the interband spin-dependent exchange interaction.[3–5] These spin-dependent interactions inside a SQD enable the spin-plasmon coupling in a SQD-MNP molecule. Theoretically, some aspects of the coherent interaction between spin states of exciton in a self-assembled SQD and plasmons at zero magnetic field were considered in a letter.[18] In contrast to Ref. 18, we calculate here important effects of the external magnetic field and consider special structures with broken symmetry. In our systems, two spin states of exciton interact, the spin splitting in the exciton spectrum can be changed, and the magnetic field controls a spin orientation of excitons.

Presently there is a lot of interest in fabrication and technology of various hybrid semiconductor-metal nanostructures having simultaneously exciton and plasmon resonances. Such solid-state material systems can be realized involving epitaxial, self-assembled, and colloidal nanostructures.[24,36–39] A layer of self-assembled SQDs can be grown in the vicinity of a crystal surface covered with metal nanocrystals.[24,37,40] Metal nanoclusters can be incorporated in a bulk crystal and can interact with bulk excitons.[38] Or, colloidal nanoparticles can be introduced into a crystal using the overgrowth method.[41] Several structures modeled in this paper incorporate semiconductor self-assembled SQDs (GaAs and InAs) and spherical and elliptical metal nanocrystals (Au and In). The structures modeled here resemble the already existing systems or can be fabricated using modern technologies.

II. MODEL AND FORMALISM

We now consider a system comprising a self-assembled SQD and a MNP (Fig. 1). A SQD is located in the plane $z=0$ at the origin of coordinates. A MNP is located above and a position of its center is given by the vector **R**. This structure can be realized using self-assembled SQDs in a semiconductor matrix. Material systems successfully used for fabrication of self-assembled quantum dots include GaAs/AlGaAs,[42] InAs/GaAs,[7] and InAs/GaAsSb.[43] In an experimental system, a MNP can be attached or grown on the surface of a sample. Here, for simplicity, we assume that a dielectric matrix (GaAs or another semiconductor) occupies

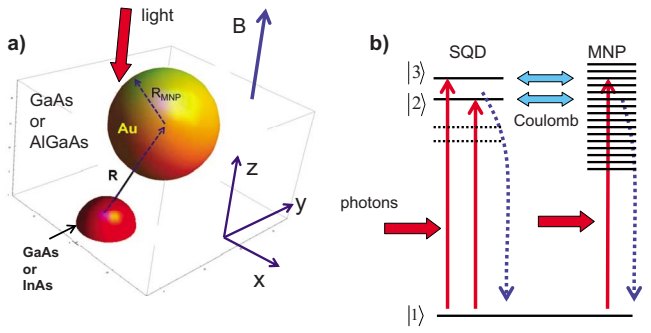

FIG. 1. (Color online) (a) Schematics of nanocrystal complex composed of semiconductor quantum dot and metal nanoparticle. (b) Transitions in the system; the vertical arrows represent light-induced transitions and relaxation in nanoparticles; the horizontal arrows depict the Coulomb interaction.

the whole three-dimensional space. In experimental structures, this situation can be obtained by covering the surface with an attached MNP by a layer of dielectric material (semiconductor or other). The case of MNP on the open surface of semiconductor should be considered separately and needs computational work because of the complex geometry. In the following, we make two approximations regarding our system. We neglect the retardation effects; in other words, we assume that our system is relatively small, $R \ll \lambda$, where λ is the wavelength if incident light. Also, we use the dipole approximation for induced electric fields inside the complex, assuming $R_{\mathrm{MNP}}, R_{\mathrm{SQD}} < R$, where R_{MNP} and R_{SQD} are the radii of MNP and SQD, respectively.

An incident electromagnetic wave approaches the system from the top and has the form: $\mathbf{E}_{ext} = \mathbf{E}_{ext,\omega} \cdot e^{-i\omega t} + \mathbf{E}^*_{ext,\omega} \cdot e^{i\omega t}$, where $\mathbf{E}_{ext,\omega} = \mathbf{e}_0 E_0$ is the complex amplitude, and $\mathbf{e}_0$ is the polarization vector and ω is the frequency. The polarization vector $\mathbf{e}_0$ is in the x-y plane and the wave vector $\mathbf{k} \| -\hat{\mathbf{z}}$. In addition, the system experiences an external magnetic field, $\mathbf{B}$, applied in the z direction. An anisotropic SQD has a shape of a lens and its spectrum consists of four excitonic states with different spin wave functions [Fig. 1(b)]. These states are formed due to interband exchange interaction. At $B=0$, two upper spin states are bright, whereas two lower states are dark. Also, the bright states at $B=0$ have optical dipoles in the x and y directions.[4] In the following, we will label the bright states as $|2\rangle$ and $|3\rangle$, whereas $|1\rangle$ will denote the ground state of the system. Here we will consider only bright states, assuming that the size of our complex (R) is longer than the exciton dimensions.[44] A spectrum of MNP is continuous and exhibits plasmon resonances. SQD and MNP interact via the Coulomb forces [Fig. 1(b)].

The equation of motion of the density matrix written for the excitons in the SQD has the form

$$\hbar \frac{\partial \rho_{nm}}{\partial t} = i\langle n|[\hat{\rho}, \hat{H}_0 + \hat{V}]|m\rangle - \sum_{kl} \Gamma_{nm,kl}\rho_{kl}, \tag{1}$$

where $|n\rangle$ are the involved quantum states, the Hamiltonian $\hat{H}_0 + \hat{V}$ consists of the internal energy of SQD ($\hat{H}_0$) and the light-matter interaction,

$$\hat{V} = -e\mathbf{r} \cdot \mathbf{E}_{tot} = |e|(\mathbf{r} \cdot \mathbf{E}_{\omega,tot} \cdot e^{-i\omega t} + \mathbf{r} \cdot \mathbf{E}^*_{\omega,tot} \cdot e^{i\omega t})$$
$$= \hat{V}_\omega \cdot e^{-i\omega t} + \hat{V}^+_\omega \cdot e^{i\omega t}, \tag{2}$$

where $\mathbf{E}_{\omega,tot}$ is the electric field acting on the exciton dipoles in the SQD. The relaxation matrix has the following elements: $\Gamma_{12,12} = \Gamma_{21,21} = \gamma_{12}$, $\Gamma_{13,13} = \Gamma_{31,31} = \gamma_{13}$, $\Gamma_{22,22} = -\Gamma_{11,22} = \gamma_{22}$, and $\Gamma_{33,33} = -\Gamma_{11,33} = \gamma_{33}$. We neglect here the spin relaxation between exciton states; such relaxation is typically slow compared to the radiative recombination and dephasing.[45] It is important to note that Eq. (1) involves plasmon excitations of MNP through the electric field,

$$\mathbf{E}_{\omega,tot} = \mathbf{E}_{\omega,ind} + \mathbf{E}_{\omega,\mathrm{MNP1}}, \tag{3}$$

where $\mathbf{E}_{\omega,ind}$ is the external field inside a SQD in the presence of a MNP. The field $\mathbf{E}_{\omega,\mathrm{MNP1}}$ describes a "self-action" of the exciton dipole and comes from the surface changes in MNP induced by the exciton dipole. The interband matrix elements of the operator $\hat{V}_\omega = |e|\mathbf{r} \cdot \mathbf{E}_{\omega,tot}$ include the vectors $\mathbf{r}_{21} = \langle 2|\mathbf{r}|1\rangle$ and $\mathbf{r}_{31} = \langle 3|\mathbf{r}|1\rangle$ which involve spin-dependent Bloch functions of excitons.[4] In Appendix A, we write down these Bloch wave functions. The matrix elements calculated with these functions have the form

$$\mathbf{r}_{21} = \langle 2|\mathbf{r}|1\rangle = \frac{r_{cv}}{\sqrt{2}}\left[\begin{pmatrix} 1 \\ -i \end{pmatrix} F^*_2 + \begin{pmatrix} 1 \\ i \end{pmatrix} G^*_2\right],$$

$$\mathbf{r}_{31} = \langle 3|\mathbf{r}|1\rangle = \frac{r_{cv}}{\sqrt{2}}\left[\begin{pmatrix} 1 \\ -i \end{pmatrix} F^*_3 + \begin{pmatrix} 1 \\ i \end{pmatrix} G^*_3\right]. \tag{4}$$

The exciton energies $E_{12(13)}$ include the interband energy contributions and the spin-dependent term,

$$E_{1j} = E_{\mathrm{SQD}} + \delta E_{spin,1j}(B),$$

where the spin-state index $j = 2, 3$, $\delta E_{spin,1j}$ is the spin energy (Appendix A), and E_{SQD} contains the band-gap and size-quantization energies of the carriers. For simplicity, we omit here a quadratic diamagnetic effect in the interband energies E_{1j}. At $B=0$, the splitting between the spin states

$$\Delta_0 = E_{12} - E_{13}.$$

In the absence of the retardation effects, the electric field $\mathbf{E}_{\omega,ind}$ is given by

$$\mathbf{d}_{\mathrm{MNP}} = E_0(\hat{\boldsymbol{\beta}}\mathbf{e}_0), \quad \mathbf{E}_{\omega,ind} = E_0\left\{\mathbf{e}_0 + \frac{3[(\hat{\boldsymbol{\beta}}\mathbf{e}_0) \cdot \mathbf{n}] \cdot \mathbf{n} - \hat{\boldsymbol{\beta}}\mathbf{e}_0}{R^3}\right\}$$
$$= E_0(\hat{\mathbf{T}} \cdot \mathbf{e}_0),$$

$$\hat{\mathbf{T}} = \begin{pmatrix} T_{xx} & T_{xy} & T_{xz} \\ T_{yx} & T_{yy} & T_{yz} \\ T_{zx} & T_{zy} & T_{zz} \end{pmatrix},$$

where $\mathbf{d}_{\mathrm{MNP}}$ is the MNP dipole moment and $\hat{\boldsymbol{\beta}}$ is the polarizability tensor of MNP; $\mathbf{n} = \mathbf{R}/R$. For an elliptical MNP, the tensor $\hat{\boldsymbol{\beta}}$ is given in Appendix B. An important case of spherical MNP is described by

$$\mathbf{E}_{\omega,ind} = E_0\left[\mathbf{e}_0 + \beta\frac{3(\mathbf{e}_0\cdot\mathbf{n})\cdot\mathbf{n}-\mathbf{e}_0}{R^3}\right], \quad \beta = R^3_{\mathrm{MNP}}\frac{\varepsilon_m-\varepsilon_0}{(2\varepsilon_0+\varepsilon_m)}, \tag{5}$$

where $\varepsilon_m=\varepsilon_m(\omega)$ and ε_0 are the dielectric constants of metal and matrix, respectively. Dielectric constants of metals (Au and In) will be taken from the empirical tables.[46] For the dielectric constant of the matrix (GaAs), we will use $\varepsilon_0=12$. Another important contribution to the field, $\mathbf{E}_{\omega,\mathrm{MNP1}}$, depends on the induced exciton dipole moment, $\mathbf{d}_\omega$, and has the form

$$\mathbf{E}_{\omega,\mathrm{MNP1}} = \frac{3(\{\hat{\boldsymbol{\beta}}\cdot[3(\mathbf{d}_{\omega,exc}\cdot\mathbf{n})\cdot\mathbf{n}-\mathbf{d}_{\omega,exc}]\}\cdot\mathbf{n})\cdot\mathbf{n}-\hat{\boldsymbol{\beta}}\cdot[3(\mathbf{d}_{\omega,exc}\cdot\mathbf{n})\cdot\mathbf{n}-\mathbf{d}_{\omega,exc}]}{\varepsilon_0 R^6} = \hat{\mathbf{A}}\cdot\mathbf{d}_{\omega,exc},$$

$$\hat{\mathbf{A}} = \begin{pmatrix} A_x^{(x)} & A_x^{(y)} & A_x^{(z)} \\ A_y^{(x)} & A_y^{(y)} & A_y^{(z)} \\ A_z^{(x)} & A_z^{(y)} & A_z^{(z)} \end{pmatrix},$$

where $\mathbf{d}_{exc}$ is the optical dipole moment of exciton (see below); $\mathbf{d}_{exc}\perp\hat{\mathbf{z}}$. Then, the light-exciton interaction operator is

$$V_{\omega,j1} = \langle j|\hat{V}_\omega|1\rangle = |e|(\mathbf{E}_{\omega,tot}\cdot\mathbf{r}_{j1}),$$

where $\mathbf{r}_{j1}=\langle j|\mathbf{r}|1\rangle$ are interband matrix elements and $j=2,3$. In the rotating-wave approximation[47]

$$\rho_{22}=\sigma_{22}, \quad \rho_{33}=\sigma_{33}, \quad \rho_{21}=\sigma_{21}e^{-i\omega t}, \quad \rho_{31}=\sigma_{31}e^{-i\omega t}. \tag{6}$$

The induced dipole moment of SQD can be written via the density matrix,

$$\mathbf{d}_{\omega,exc} = -|e|(\sigma_{21}\cdot\mathbf{r}_{12}+\sigma_{31}\cdot\mathbf{r}_{13}).$$

In the linear regime, the diagonal matrix elements are given by

$$\rho_{22} = i\frac{\sigma_{21}\cdot V^+_{\omega,12}-V_{\omega,21}\cdot\sigma_{12}}{\gamma_{22}},$$

$$\rho_{33} = i\frac{\sigma_{31}\cdot V^+_{\omega,13}-V_{\omega,31}\cdot\sigma_{13}}{\gamma_{33}}.$$

For the nondiagonal elements, we obtain

$$\sigma_{21} = \frac{[\hbar\omega-E_{13}+i\gamma_{13}+e^2\mathbf{r}_{31}\cdot(\hat{\mathbf{A}}\cdot\mathbf{r}_{13})]|e|(\mathbf{r}_{21}\cdot\mathbf{E}_{\omega,ind})-|e|^3(\mathbf{r}_{31}\cdot\mathbf{E}_{\omega,ind})[\mathbf{r}_{21}\cdot(\hat{\mathbf{A}}\cdot\mathbf{r}_{13})]}{[\hbar\omega-E_{13}+i\gamma_{13}+e^2\mathbf{r}_{31}\cdot(\hat{\mathbf{A}}\cdot\mathbf{r}_{13})][\hbar\omega-E_{12}+i\gamma_{12}+e^2\mathbf{r}_{21}\cdot(\hat{\mathbf{A}}\cdot\mathbf{r}_{12})]-e^4[\mathbf{r}_{31}\cdot(\hat{\mathbf{A}}\cdot\mathbf{r}_{12})][\mathbf{r}_{21}\cdot(\hat{\mathbf{A}}\cdot\mathbf{r}_{13})]},$$

$$\sigma_{31} = \frac{[\hbar\omega-E_{12}+i\gamma_{12}+e^2\mathbf{r}_{21}\cdot(\hat{\mathbf{A}}\cdot\mathbf{r}_{12})]|e|(\mathbf{r}_{31}\cdot\mathbf{E}_{\omega,ind})-|e|^3(\mathbf{r}_{21}\cdot\mathbf{E}_{\omega,ind})[\mathbf{r}_{31}\cdot(\hat{\mathbf{A}}\cdot\mathbf{r}_{12})]}{[\hbar\omega-E_{13}+i\gamma_{13}+e^2\mathbf{r}_{31}\cdot(\hat{\mathbf{A}}\cdot\mathbf{r}_{13})][\hbar\omega-E_{12}+i\gamma_{12}+e^2\mathbf{r}_{21}\cdot(\hat{\mathbf{A}}\cdot\mathbf{r}_{12})]-e^4[\mathbf{r}_{31}\cdot(\hat{\mathbf{A}}\cdot\mathbf{r}_{12})][\mathbf{r}_{21}\cdot(\hat{\mathbf{A}}\cdot\mathbf{r}_{13})]}.$$

The absorption rate from the system (SQD and MNP) is given by[13,48]

$$Q = Q_{\mathrm{SQD}} + Q_{\mathrm{MNP}}, \tag{7}$$

where

$$Q_{\mathrm{SQD}} = E_{12}\sigma_{22}\gamma_{22} + E_{13}\sigma_{33}\gamma_{33},$$

$$Q_{\mathrm{MNP}} = \int_{V_{\mathrm{NP}}} dV\mathbf{j}\cdot\mathbf{E} = \mathrm{Im}(\varepsilon_{\mathrm{NP}})\frac{\omega}{2\pi}\int_{V_{\mathrm{NP}}} dV\mathbf{E}^{in}_{\omega}\cdot\mathbf{E}^{in*}_{\omega}, \tag{8}$$

where the electric current inside a MNP is given by $\mathbf{j}_\omega=-i\omega(\varepsilon_m-1)/4\pi\cdot\mathbf{E}^{in}_\omega$. Also, $\mathbf{E}^{in}_\omega=\mathbf{E}^{in}_{\omega,ind}+\mathbf{E}^{in}_{\omega,exc}$, where $\mathbf{E}^{in}_{\omega,ind}$ and $\mathbf{E}^{in}_{\omega,exc}$ are the fields inside the MNP induced by the external radiation and by the oscillating exciton dipole, respectively. Since the dissipation rate is a positive value, the above equations assume that $\mathrm{Im}(\varepsilon_{\mathrm{NP}})>0$. In the dipole approach, the field $\mathbf{E}^{in}_{\omega,ind}$ has the form

$$\mathbf{E}^{in}_{\omega,ind} = \hat{\boldsymbol{\gamma}}\cdot\left\{E_0\mathbf{e}_0 + \frac{[3(\mathbf{d}_{\omega,exc}\cdot\mathbf{n})\cdot\mathbf{n}-\mathbf{d}_{\omega,exc}]}{R^3}\right\},$$

where the tensor $\hat{\boldsymbol{\gamma}}$ couples the uniform external field and the field inside a metal ellipsoid (Appendix B). For a spherical

MNP, $\hat{\boldsymbol{\gamma}}=[3\varepsilon_0/(2\varepsilon_0+\varepsilon_m)]\hat{\mathbf{1}}$. The MNP dissipation can be reduced to

$$Q_{\mathrm{MNP}}=\frac{2\omega}{3}R_{\mathrm{MNP}}^3|\mathbf{E}_{\omega}^{in}|^2\mathrm{Im}[\varepsilon_m].$$

The resultant total dissipation $Q=Q_{\mathrm{SQD}}+Q_{\mathrm{MNP}}$ includes the effects of interference between three terms in the electric field: The external electromagnetic wave, the field induced by surface changes in MNP, and the field due to the optically driven excitonic dipoles of SQD. The cross section of optical absorption is then calculated as

$$\sigma=\frac{Q}{I_0}=\frac{2\pi}{c_0\sqrt{\varepsilon_0}\cdot E_0^2}Q.$$

The formalism based on the master equation [Eq. (1)] treats rigorously the nonretarded (near-field) Coulomb interaction between the exciton and plasmon. But, the coupling of the exciton with the electrometric waves is only included via the phenomenological broadening γ_{1j}. In the absence of MNP, $\gamma_{1j}^0=\gamma_{rad,0}/2+\gamma_{\mathrm{dephasing}}$, where $\gamma_{rad,0}=\hbar/\tau_0$, τ_0 is the radiative lifetime, and $\gamma_{\mathrm{dephasing}}$ is the broadening due to internal dephasing in a SQD. In the presence of MNP, the phenomenological broadenings in Eq. (1) become $\gamma_{1j}=p_j\cdot(\gamma_{rad,0}/2)+\gamma_{\mathrm{dephasing}}$, where p_j are plasmon enhancement factors. Simultaneously, the total broadening of exciton resonance in the presence of metal nanocrystal acquires a term due to nonradiative energy transfer, $\gamma_{\mathrm{FRET},j}$. This energy-transfer mechanism comes from dissipation of energy of oscillating exciton dipole inside the metal component. Then, the total broadening is given by $\gamma_{1j}^{tot}=p_j\cdot(\gamma_{rad}/2)+\gamma_{\mathrm{dephasing}}+\gamma_{\mathrm{FRET},j}$. In Sec. III, we model nanostructures with small radiative broadenings: $\gamma_{1j}^{tot}\gg p_j\cdot(\gamma_{rad}/2)$ or $\gamma_{\mathrm{dephasing}}+\gamma_{\mathrm{FRET},j}>p_j\cdot(\gamma_{rad}/2)$. In other words, the radiative broadening for the nanostructures studied in Sec. III can be neglected. In general, we should note that the quantum formalism based on Eq. (1) is valid for relatively small nanostructures in which the radiative damping is smaller than the other broadenings (internal dephasing and energy-transfer broadening). For example, a MNP with a large size (~photon wavelength) acquires a large radiative broadening of a plasmon resonance due to strong coupling with photons.[20] Our formalism cannot describe this case but it describes consistently small structures with a small radiative damping.

III. APPLICATIONS

A. Plasmon-induced interaction between spin states of exciton

The eigenenergies of the exciton states in a SQD-MNP molecule in the presence of the exciton-plasmon Coulomb interaction can be obtained from the spectrum of energy dissipation inside a SQD: $Q_{\mathrm{SQD}}(\omega)$. In our model, this spectrum has two peaks as a function of ω. Considering ω as a complex variable, the function $Q_{\mathrm{SQD}}(\omega)$ has two poles with the positions given by

$$[\hbar\omega-E_{13}+i\gamma_{13}+e^2\mathbf{r}_{31}\cdot(\hat{\mathbf{A}}\cdot\mathbf{r}_{13})][\hbar\omega-E_{12}+i\gamma_{12}+e^2\mathbf{r}_{21}\cdot(\hat{\mathbf{A}}\cdot\mathbf{r}_{12})]-e^4[\mathbf{r}_{31}\cdot(\hat{\mathbf{A}}\cdot\mathbf{r}_{12})][\mathbf{r}_{21}\cdot(\hat{\mathbf{A}}\cdot\mathbf{r}_{13})]=0. \quad (9)$$

To solve Eq. (9), we first note that the tensor $\hat{\mathbf{A}}$ is a slow function of ω because the metal dielectric function has typically very broad spectral structures. Therefore, we treat here $\hat{\mathbf{A}}$ as a constant: $\hat{\mathbf{A}}=\hat{\mathbf{A}}(\omega=\omega_0)$. Then, we find the complex roots of Eq. (9),

$$\hbar\Omega_{12(13)}=\frac{\tilde{E}_{13}+\tilde{E}_{12}\pm\sqrt{(\tilde{E}_{12}-\tilde{E}_{13})^2+4E_{\mathrm{int}}^2}}{2},$$

$$\tilde{E}_{12}=E_{12}-i\gamma_{12}-e^2\mathbf{r}_{21}\cdot(\hat{\mathbf{A}}\cdot\mathbf{r}_{12}),\quad \tilde{E}_{13}=E_{13}-i\gamma_{13}-e^2\mathbf{r}_{31}\cdot(\hat{\mathbf{A}}\cdot\mathbf{r}_{13}),\quad \tilde{E}_{\mathrm{int}}^2=e^4[\mathbf{r}_{31}\cdot(\hat{\mathbf{A}}\cdot\mathbf{r}_{12})]\times[\mathbf{r}_{21}\cdot(\hat{\mathbf{A}}\cdot\mathbf{r}_{13})]. \quad (10)$$

The imaginary parts of $\hbar\Omega_{1j}$ give the decays of excitons, whereas the real parts are the Lamb shifts of energies due to the exciton-plasmon interaction. The positions of the peaks of $Q_{\mathrm{SQD}}(\omega)$ are close to $\hbar\,\mathrm{Re}[\Omega_{12(13)}]$. The interaction between the two spin states of the exciton is given by the parameter $\tilde{E}_{\mathrm{int}}$. The parameter $\tilde{E}_{\mathrm{int}}$ is nonzero if a SQD-MNP system has reduced symmetry or in the presence of a magnetic field. We now consider two particular cases. If a SQD-MNP system has one of two particular planes of symmetry (x-z or y-z plane), the matrix $\hat{\mathbf{A}}$ is diagonal and the interaction between two excitons exists only in the presence of a magnetic field,

$$\tilde{E}_{\mathrm{int}}^2=e^4(x_{31}A_x^{(x)}x_{12}+y_{31}A_y^{(y)}y_{12})(x_{21}A_x^{(x)}x_{13}+y_{21}A_y^{(y)}y_{13}).$$

This equation is nonzero only if $B\neq 0$ since, at $B=0$, the exciton dipoles ($\mathbf{r}_{12}$ and $\mathbf{r}_{13}$) are linearly polarized in the x and y directions. At $B=0$, the parameter $\tilde{E}_{\mathrm{int}}$ does not vanish if a SQD-MNP system has lowered symmetry mentioned above (also see Fig. 6 below). Then, $\tilde{E}_{\mathrm{int}}^2=e^4(y_{31}A_y^{(x)}x_{12})(x_{21}A_x^{(y)}y_{13})$.

B. GaAs/GaAlAs quantum dot and spherical Au nanoparticle

Figure 2(a) shows the chosen geometry for the system. At $B=0$, the excitons of SQD have optical dipoles along the x and y directions. A MNP is located on the x axis and its radius $R_{\mathrm{MNP}}=7.5$ nm. The distance between a SQD and a MNP is $R=20$ nm and the vector $\mathbf{n}=\mathbf{R}/R=(1/\sqrt{2},0,1/\sqrt{2})$. The vertical distance between the SQD and the MNP surface $d\sim 6.6$ nm. The dielectric constant of matrix $\varepsilon_0=12$ and the Au constant is taken from Ref. 46. The dipole approximation for the exciton-plasmon interaction is valid for an exciton located at sufficiently long distance ΔR from the surface of MNP. In particular, the dipole approximation is applicable if $\Delta R>R_{\mathrm{MNP}}$. In our geometry, $\Delta R=12.5$ nm and the dipole condition is satisfied. The exciton energy is chosen typical for a GaAs/GaAlAs self-assembled dot,[42] $\hbar\omega_0=1.6$ eV. The interband dipole used here describes optical transitions in

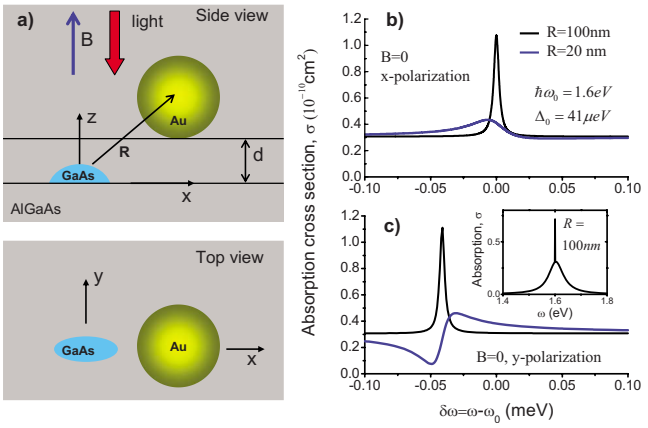

FIG. 2. (Color online) (a) Model and geometry of a complex composed of spherical gold nanoparticle and GaAs quantum dot. [(b) and (c)] Optical absorption spectra for two polarizations of incident light and for two distances $R=100$ and 20 nm. Inset shows the absorption of the complex in a wide energy interval.

GaAs: $r_{cv}=6.5$ Å. Then, the bare exciton energies at $B=0$ are denoted as: $E_{12}=\hbar\omega_0$ and $E_{13}=\hbar\omega_0-\Delta_0$. An exchange splitting Δ_0 and other microscopic parameters of the Hamiltonian vary from dot to dot and, here, we will use some typical realistic numbers for these parameters.[4,7] The exchange-splitting energy in self-assembled SQDs is relatively small and will be chosen here as $\Delta_0=0.75|b_x-b_y|=41$ μeV. Other parameters, including g factors, will be: $a_z=-0.2$, $b_z=-0.2$, $b_x=0.155$, $b_y=0.1$, $g_e=-0.8$, and $g_h=-2.2$.

Figures 2(b) and 2(c) show calculated absorption spectra of SQD-MNP molecule for $R=20$ and 100 nm. For convenience, we plot the absorption spectrum as a function of the detuning from the high-energy exciton peak, $\hbar\delta\omega=\hbar(\omega-\omega_0)$, where $\hbar\omega_0=E_{12}(B=0)$. At low temperatures (~4 K), the intrinsic broadening of isolated dipole, γ^0_{1j}, is rather small.[7,31] For our calculations, we take the following numbers: $\gamma^0_{1j}=2.2$ μeV and $\tau^0_{rad}=1$ ns. At long separations R, the effect of MNP on the absorption in a SQD is weak and the absorption spectra show two Lorentzian peaks. For the x-polarized incident wave, the peak is located at $E_{12}=\hbar\omega_0$ and, for the y-polarized incident wave, the peak is centered at $E_{13}=\hbar\omega_0-\Delta_0$. This is in agreement with the selection rules for the spin states of excitons.[4] For $R=20$ nm, the exciton-plasmon interaction strongly modifies the spectrum. First, the lines acquire Fano line shapes. This effect happens mainly due to the interference between the incident electric field and the exciton-induced dipole field. Mathematically, this effect comes from the function $Q_{\rm MNP}$ [Eq. (8)] which incorporates the interfering fields, $\mathbf{E}_{\omega,ind}$ and $\mathbf{E}_{\omega,exc}$. In addition, the positions of the lines become shifted and are given now by $\hbar\Omega_{12(13)}$ [Eq. (10)]. We also note that the optical selection rules for the x and y excitons are not changed in this SQD-MNP molecule because the exciton-plasmon interaction does alter the symmetry of the SQD in this geometry. The system still has a symmetry plane (z-x plane). However, in a high magnetic field, optical selection rules become strongly altered by the exciton-plasmon interaction (Fig. 3). In strong magnetic fields ($|\Delta E_Z| \gg \Delta_0$), the spectral lines of SQD in the

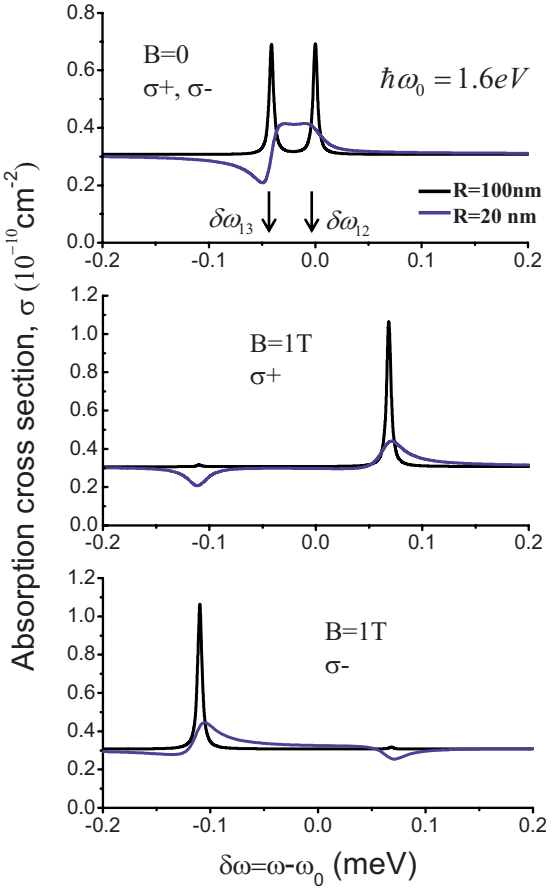

FIG. 3. (Color online) Optical absorption spectra of Au-GaAs complex in the presence of an external magnetic field. The geometry of this complex is shown in Fig. 2(a).

absence of MNP are circularly polarized. For the σ_+ polarization of incident light $[\mathbf{e}_0^{(+)}=(\mathbf{x}+i\mathbf{y})/\sqrt{2}]$, the absorption process involves only the high-energy exciton (E_{12}), whereas, for the σ_- excitation $[\mathbf{e}_0^{(-)}=(\mathbf{x}-i\mathbf{y})/\sqrt{2}]$, the spectrum includes only the excitation E_{13}. In the presence of MNP, these traditional selection rules break down because the MNP disturbs the cylindrical symmetry of the exciton states in high magnetic fields. In the presence of the exciton-plasmon interaction, the normally forbidden transitions (E_{13} for σ_+ excitation and E_{12} for σ_- excitation) become now allowed and, interestingly, appear in the spectra as antiresonances (Fig. 3). The appearance of these transitions in the form of antiresonance can be understood as an effect of interference of electric fields inside the MNP. These electric fields are the incident circularly polarized wave and the dipole fields induced by the spin-polarized excitons. Mathematically, antiresonances come from the function $Q_{\rm MNP}$.

It is also interesting to look at the shifts of exciton energies in the presence of a MNP. For our geometry at $B=0$, the exciton states are not mixed. The plasmon-induced (Lamb) shifts of excitons can be taken from the formulas for $\tilde{E}_{1j}$ [Eq. (10)],

$$\delta E_{1j}^{Lamb} = \tilde{E}_{1j} - E_{1j} + i\gamma_{1j} = -e^2 \mathbf{r}_{j1} \cdot (\hat{\mathbf{A}} \cdot \mathbf{r}_{1j}),$$

where $j=2,3$. The real part of δE_{1j}^{Lamb} can be positive or negative [Fig. 4(a)]. The parameter $-\mathrm{Im}[\delta E_{1j}^{Lamb}]$ should be

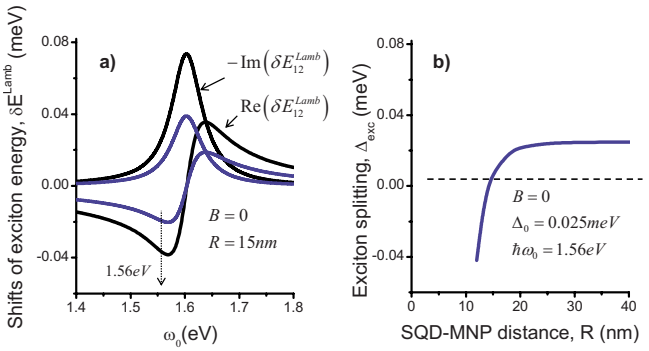

FIG. 4. (Color online) (a) Calculated shifts of exciton energies and broadenings for the Au-GaAs complex shown in Fig. 2(a). The curves of two colors are given for the excitons $\hbar\Omega_{12}$ and $\hbar\Omega_{13}$, respectively. (b) The exciton splitting in the same complex as a function of SQD-MNP distance.

positive since it describes energy transfer from excitons to plasmons [Fig. 4(a)]. One can see that the exciton-plasmon interaction can create significant shifts of exciton energies. In our geometry, the x and y excitons interact differently with the plasmon subsystem and, therefore, the exciton splitting at $B=0$,

$$\Delta_{exc} = \hbar\Omega_{12} - \hbar\Omega_{13},$$

should depend on the SQD-MNP distance, R. Now we look at the function $\Delta_{exc}(R)$ for the exciton energy $\hbar\omega_0 = 1.56$ eV. At this energy, the Lamb shifts are strong and negative [Fig. 4(a)] and, simultaneously, the dissipation of the excitons is relatively weak. Figure 4(b) shows the exciton splitting as a function of R. Interestingly, Δ_{exc} vanishes at $R \sim 14$ nm. Here we took a smaller number for the internal exchange splitting, $\Delta_0 = 25$ μeV; the corresponding exchange parameters were $b_x = 0.134$ and $b_y = 0.1$. A spectrum of exciton-plasmon excitations in a magnetic field is shown in Fig. 5. We plot here the energies

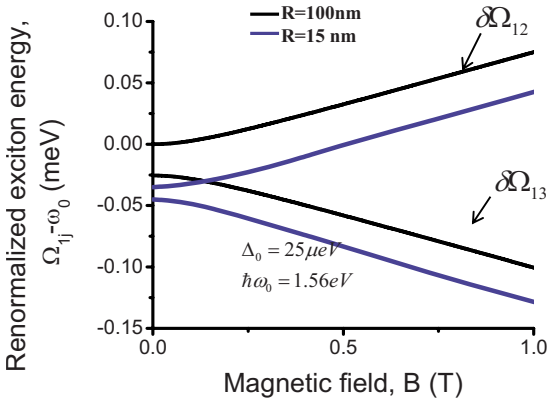

FIG. 5. (Color online) The energies of excitons in the Au-GaAs complex. Blue curves show the renormalization of the energies and the reduction in the spin splitting due to the exciton-plasmon interaction in the complex with $R=20$ nm [Fig. 2(a)].

$$\hbar\delta\Omega_{1j} = \hbar\Omega_{1j} - \hbar\omega_0$$

for $R=15$ and $R=100$ nm. One can see that, at $R=15$ nm, the zero-magnetic-field exchange splitting becomes strongly reduced due to the exciton-plasmon interaction. This is an example of a spin-dependent interaction between excitons and plasmons.

It is interesting to compare our results with the results of Ref. 14. The paper[14] describes the interaction between excitons and plasmons in hybrid structures composed of molecules and metal nanocrystals. Several optically active molecules (J-aggregates) form a shell around a metal nanocrystal. The molecule system in this structure exhibits a strong collective exciton resonance in the optical spectra. In this situation, the excitons strongly interact with the plasmons and this interaction appears in a form of Rabi splitting. In our structures, we have a different regime of interaction. Our system includes single exciton lines with relatively weak oscillator strengths. In addition, the exciton in our system has a very narrow absorption line (this assumes low temperatures), whereas the plasmon resonance is very broad. The integrated absorption of the plasmon peak is much greater than that of the exciton. This physical situation corresponds to the regime of Fano effect. In this regime, exciton peaks in the absorption spectra acquire asymmetric shapes and also become shifted and broadened.

C. InAs/GaAs quantum dot and Au nanorod

We now consider a system with a gold nanorod in a geometry shown in Fig. 6(a). The parameters are: $R=26$ nm and $\mathbf{n}=(1/2,1/2,1/\sqrt{2})$. A nanorod is taken in the form of ellipsoid with dimensions: $R_{\mathrm{MNP}x}=15$ nm, and $R_{\mathrm{MNP}y} = R_{\mathrm{MNP}z}=8.5$ nm, where $R_{\mathrm{MNP}i}$ is the radius of the ellipsoid in the i direction. This nanorod has two plasmon resonances and one of them is at ~ 1.2 eV [inset of Fig. 6(c)]. This is the typical energy of excitons in InAs/GaAs self-assembled dots.[7] According to the selection rules, the x-polarized light creates only the high-energy exciton peak (x exciton) for long R [Fig. 6(b)]. For shorter SQD-MNP separations, one can see the y exciton as antiresonance in this spectrum because the exciton-plasmon interaction breaks the symmetry of the system and the y exciton becomes active under the x-polarized excitation. We also can see that the exciton with the x dipole interacts weakly with the x plasmon because the electric field of this exciton dipole at the center of MNP ($\mathbf{r}=\mathbf{R}$) lies approximately in the zy plane. Simultaneously, the direction of the electric field of the y dipole at $\mathbf{r}=\mathbf{R}$ is close to the x direction and, therefore, the interaction of the y exciton with the x plasmon is strong and appears in the absorption spectrum as a Fano-type antiresonance [Fig. 6(b)]. Again, mathematically, the antiresonance comes from the function $Q_{\mathrm{MNP}}(\omega)$ and originates from the interference of the electric fields inside a MNP. Simultaneously, the dissipation inside a SQD (Q_{SQD}) shows just two peaks and, of course, has not antiresonances [Fig. 6(c)] and, in the presence of a MNP, the second peak due to the y exciton appears in the function Q_{SQD} [see Fig. 6(c) for $R=26$ nm] due to the breaking of symmetry in the system. This is another example of

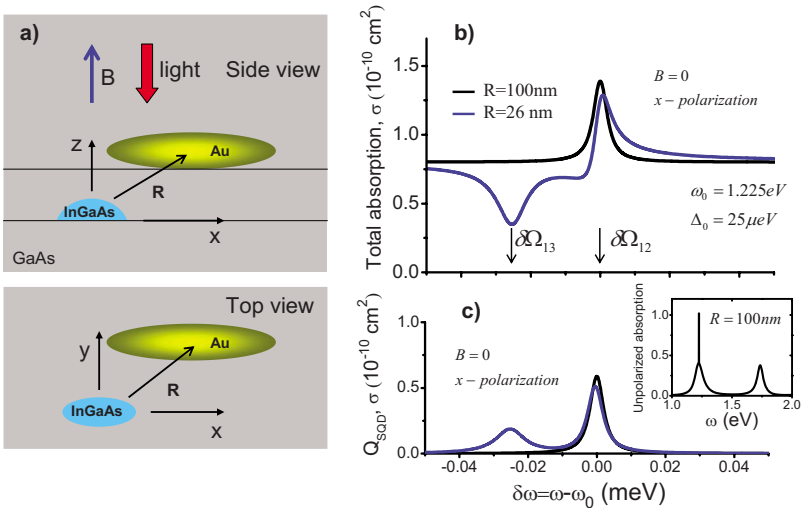

FIG. 6. (Color online) (a) Model and geometry of the complex composed of gold nanorod and GaAs quantum dot. (b) Optical absorption spectra for the x polarization of incident light and for two distances $R=100$ and 26 nm. (c) Optical absorption by the quantum dot Q_{SQD} in the complex. Inset shows the absorption of the complex in a wide energy interval.

modification of selection rules for the SQD excitons in the presence of the exciton-plasmon interaction.

IV. PHOTOLUMINESCENCE (PL) IN A MAGNETIC FIELD

A. Rate equation formalism

In Sec. IV, we will neglect the coherent components of the exciton-plasmon interaction and consider simple classical rate equations describing the incoherent exciton dynamics. In the quantum-mechanical approach, the processes of absorption and emission are described with the operator of light-dipole interaction,[49]

$$\hat{V}_{\mathrm{int}} = -e\mathbf{r}\cdot\hat{\mathbf{E}}_0 = i|e|\mathbf{r}\cdot\sum_{k,\alpha}\sqrt{\frac{2\pi\hbar\omega_k}{\varepsilon_0 V}}(\mathbf{e}_k^{(\alpha)}\hat{c}_{k,\alpha}e^{-i\omega_k t} - \mathbf{e}_k^{(\alpha)*}\hat{c}_{k,\alpha}^{+}e^{i\omega_k t}), \tag{11}$$

where $\mathbf{k}$ and α are the photon wave vector and the photon polarization index, respectively. For circularly polarized photons with a wave vector along the z direction, $\mathbf{e}_k^{(\alpha=\pm)} = (\hat{\mathbf{x}} \pm i\hat{\mathbf{y}})/\sqrt{2}$. In the presence of a MNP, a local electromagnetic field at the SQD becomes modified in the way similar to the modification $\mathbf{E}_{\omega,ext} \to \mathbf{E}_{\omega,ind}$, as it was already calculated. Then, the polarization vector in Eq. (11) should be changed,

$$\mathbf{e}_k^{(\alpha)} \to \tilde{\mathbf{e}}_k^{(\alpha)} = \left\{\mathbf{e}_k^{(\alpha)} + \frac{3[(\hat{\boldsymbol{\beta}}\mathbf{e}_k^{(\alpha)})\cdot\mathbf{n}]\cdot\mathbf{n} - \hat{\boldsymbol{\beta}}\mathbf{e}_k^{(\alpha)}}{R^3}\right\} = \hat{\mathbf{T}}\cdot\mathbf{e}_k^{(\alpha)}. \tag{12}$$

This leads to strongly modified absorption and emission matrix elements. The absorption process in the presence of a MNP was described above using a classical electromagnetic field. In particular, the classical field $\mathbf{E}_{\omega,ind} \propto \hat{\mathbf{T}}\cdot\mathbf{e}_0$ entered the matrix elements of the light-matter interaction $(\mathbf{r}_{j1}\cdot\mathbf{E}_{\omega,ind})$ in the density matrix (see the equations for σ_{j1}). The quantum approach to the electromagnetic field [Eqs. (11) and (12)] gives the following optical matrix element $\mathbf{r}_{j1}\cdot(\hat{\mathbf{T}}\cdot\mathbf{e}_k^{(\alpha)})$; this is similar to the previously used matrix elements, $\mathbf{r}_{j1}\cdot\mathbf{E}_{\omega,ind} \propto \mathbf{r}_{j1}\cdot(\hat{\mathbf{T}}\cdot\mathbf{e}_0)$, calculated with the classical field.

We now focus on the emission process. The probability of spontaneous emission of photon with $\mathbf{k}\|\mathbf{z}$ is calculated from Eq. (11),

$$\gamma_{rad,j}^{(\alpha)} \propto |\langle 1|\mathbf{r}|j\rangle\cdot\tilde{\mathbf{e}}_k^{(\alpha)*}|^2,$$

where $\alpha=\pm$ and the vector $\langle 1|\mathbf{r}|j\rangle$ is given in Appendix A. We see now that the radiation process also becomes strongly modified because the vector $\tilde{\mathbf{e}}_k^{(\alpha)}$ includes the plasmon-induced field of MNP. Assuming a nonresonant pumping, an emission process can be described using simple rate equations,[11,26]

$$\frac{dn_j}{dt} = -(\gamma_{rad,j}^{tot} + \gamma_{\mathrm{FRET},j} + \gamma_{nonrad})n_j + I_j,$$

where n_j are the populations of the exciton states with $j=2,3$ and I_j are the rates of optical generation. The relaxation rates $\gamma_{rad,j}^{tot}$, $\gamma_{\mathrm{FRET},j}$, and γ_{nonrad} come from radiative processes, nonradiative energy transfer to a MNP, and intrinsic nonradiative recombination in a SQD, respectively. This rate-equation approach assumes that we neglect the coherent component of the exciton-plasmon interaction. In other words, the exciton-plasmon interaction should be relatively weak so that $|\Delta_0| \gg |\delta E_{1j}^{Lamb}|$. The above approximation also means that the plasmon-induced mixing between two spin states is small, i.e., $|E_{\mathrm{int}}| \ll \Delta_0$. Simultaneously, the effect of the plasmonic field on the PL spectrum can be overall strong as we will see below. Then, we can use the bare exciton energies, E_{1j}, to model the PL spectrum. Under continuous pumping, the intensity of PL line is proportional to $n_j\cdot\gamma_{rad,j}^{(\alpha)}$. Using the rate equations, we obtain n_j under the steady-state conditions and then calculate the PL spectrum for the two polarizations $\alpha=\pm$,

$$\mathrm{PL}^{(\alpha)} \propto P(\omega_{pump}) \times\left[\frac{\gamma_{rad,2}^{(\alpha)}}{\gamma_{rad,2}^{tot} + \gamma_{nonrad} + \gamma_{\mathrm{FRET},2}}\frac{\Gamma_{\mathrm{PL}}}{\Gamma_{\mathrm{PL}}^2 + (\hbar\omega - E_{12})^2} + \frac{\gamma_{rad,3}^{(\alpha)}}{\gamma_{rad,3}^{tot} + \gamma_{nonrad} + \gamma_{\mathrm{FRET},3}}\frac{\Gamma_{\mathrm{PL}}}{\Gamma_{\mathrm{PL}}^2 + (\hbar\omega - E_{13})^2}\right].$$

For simplicity, we neglected above spin-flip transitions be-

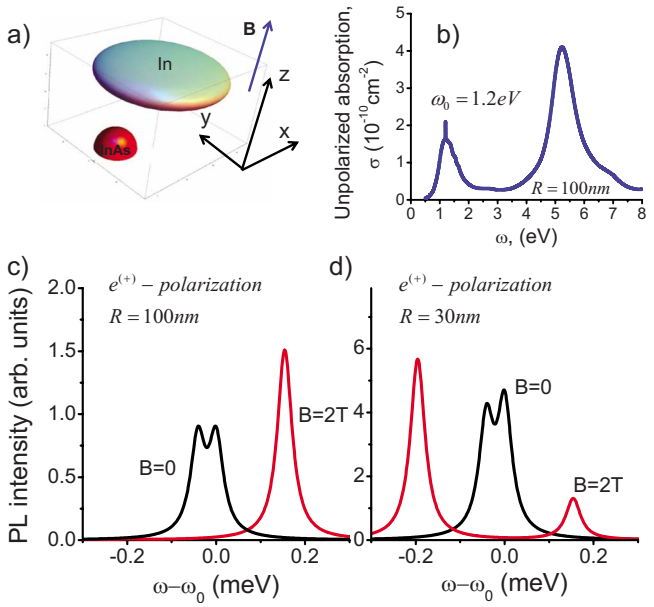

FIG. 7. (Color online) (a) Model and geometry of a hybrid In-InAs system. The system includes an InAs dot and an oblate metallic ellipsoid made of Indium. (b) Absorption spectra for the system in a wide range of photon energies. [(c) and (d)] PL spectra in the magnetic field (c) for an isolated quantum dot and (d) for a quantum dot interacting with an In nanocrystal.

tween exciton states in a SQD. The total radiative rates $\gamma_{rad,j}^{tot}=\gamma_{rad,0}P_j$, where $\gamma_{rad,0}$ is the total radiative rate of the excitons in the absence of MNP. The B-dependent factors

$$P_j=\frac{1}{2}(|(F_j+G_j)T_{xx}^*+(F_j-G_j)T_{yx}^*|^2 + |(F_j+G_j)T_{xy}^*+(F_j-G_j)T_{yy}^*|^2).$$

At $B=0$ and $R\to\infty$, these factors $P_j\to 1$. For $B=0$ and for the symmetric case [Fig. 7(a)], $P_2\to|T_{xx}|^2$ and $P_3\to|T_{yy}|^2$. The factors P_j describe the modification of the emission rates of magnetoexcitons in the presence of a MNP. The nonresonant pumping rates $I_j=I_0\cdot P(\omega_{pump})$. The factor $P(\omega_{pump})$ comes from the field enhancement of absorption of pumping light with a frequency ω_{pump} and a field $\mathbf{E}_{\omega,pump}$. For a nonresonant excitation with photon energies above the barrier material, this factor can be estimated as

$$P(\omega_{pump})=\frac{|\hat{\mathbf{T}}\cdot\mathbf{E}_{\omega,pump}|^2}{E_{\omega,pump}^2}.$$

We now consider the rate of energy transfer, $\gamma_{\mathrm{FRET}}^{(\alpha)}$. This energy-transfer process is similar to the Förster resonance energy transfer (FRET) mechanism. Then, we can use the Fermi's golden rule to calculate the rate of exciton transfer from a SQD to a MNP.[26] The resulting rates of are

$$\gamma_{\mathrm{FRET},j}=-2\cdot\mathrm{Im}[\tilde{E}_{1j}-i\gamma_{1j}]=2\cdot\mathrm{Im}[e^2\mathbf{r}_{j1}\cdot(\hat{\mathbf{A}}\cdot\mathbf{r}_{1j})],$$

where $\tilde{E}_{1j}$ are the solutions for the poles of the functions σ_{1j} in the absence of the coherent mixing between excitons [Eq. (10)]. For one simple case, the energy-transfer rates are

$$\gamma_{\mathrm{FRET},j}=2s_j\frac{e^2r_{cv}^2}{\varepsilon_0R^6}\mathrm{Im}[\beta_j].$$

To derive this equation, we assumed $B=0$ and $\mathbf{n}\|\mathbf{x}$. For $j=2$, $s_2=4$, and $\beta_j=\beta_{xx}$. In the case of $j=3$, $s_3=1$, and $\beta_3=\beta_{yy}$.

B. Magnetophotoluminescence from InAs/GaAs quantum dot and In nanocrystal

The system is now composed of InAs SQD and In MNP. The In MNP is an oblate ellipsoid with dimensions: $R_{\mathrm{MNP}x}=R_{\mathrm{MNP}y}=40$ nm and $R_{\mathrm{MNP}z}=10$ nm. The low-frequency plasmon resonance of such ellipsoid is at $\sim$1.2 eV that overlaps perfectly with the typical exciton energies of InAs SQDs.[7] Similar structures with In islands and InAs self-assembled dots were reported recently in the experimental paper.[24] In our calculations, the geometrical and other parameters are: $\mathbf{n}=(1/\sqrt{2},0,1/\sqrt{2})$, $R=30$ nm, $\varepsilon_0=12$, $\omega_0=1.2$ eV, $\Gamma_{\mathrm{PL}}=20$ μeV, $\Delta_0=41$ μeV, $\gamma_{nonrad}=\hbar/\tau_{nonrad}$, $\tau_{nonrad}=10$ ns, $\gamma_{rad,0}=\hbar/\tau_{rad,0}$, and $\tau_{rad,0}=1$ ns. The indium dielectric constant is taken from Ref. 46. For the chosen parameters, the coherent shifts of excitons can be neglected ($|\delta E_{1j}^{Lamb}|\ll\Delta_0$) because the chosen distance R is relatively long. However, the plasmon-enhancement effects remain strong. In particular, the plasmon enhancement factor $P(\omega_{pump}=1.6\ \mathrm{eV})\sim 11$ for $\mathbf{E}_{\omega,pump}\|\mathbf{x}$. This also means that the optical selection rules for the PL process can be strongly changed. Indeed, we see this effect in the calculations (Fig. 7). For long R and negligible exciton-plasmon interaction, the PL spectra in a magnetic field follow the usual selection rules [Fig. 7(c)]. At $B=0$, both excitons (x and y states) are active in the emission configuration with $\mathbf{e}_k^{(+)}$ and $\mathbf{k}\|\hat{\mathbf{z}}$. At high magnetic fields, the high-energy exciton mode dominates in the $\mathbf{e}_k^{(+)}$-emission spectrum. For shorter distances R, a MNP starts to influence strongly the electromagnetic fields of incident and emitted photons and, simultaneously, the energy-transfer process ($\gamma_{\mathrm{FRET},j}$) becomes active. And we see overall enhancement of PL together with a strong alternation of the selection rules in high magnetic fields [Figs. 7(c) and 7(d)]. Three processes affect the PL intensity: The absorption, radiative emission, and nonradiative energy transfer. The absorption rate is strongly increased: $P(\omega_{pump})\sim 11$. The radiative rates ($\gamma_{rad,j}^{(\alpha)}$ and $\gamma_{rad,j}^{tot}$) are significantly increased due to the presence of the plasmon resonance. For $R=30$ nm and $B=0$, calculated enhancement factors for these rates are: $P_2\sim 4.2$ and $P_3\sim 12$. Simultaneously, the FRET rates grow as the distance R decreases. For $R=30$ nm and $B=0$, the FRET rates become comparable with the radiation rates: $\gamma_{\mathrm{FRET},2}\sim 2.2$ μeV, $\gamma_{\mathrm{FRET},3}\sim 7.9$ μeV, $\gamma_{rad,2}^{tot}\sim 1.7$ μeV, and $\gamma_{rad,3}^{tot}\sim 4.9$ μeV. The enhanced radiative rates tend to increase the PL intensity whereas the emerging energy-transfer process tends to decrease the emission. Now we comment on the selection rules. The change in the selection rules in the magneto-PL spectra [Fig. 7(d)] comes from the exciton-plasmon interaction and from the breaking of cylindrical symmetry in the presence of an optically active MNP. In particular, the radiative rates $\gamma_{rad,2}^{(+)}$ and $\gamma_{rad,3}^{(+)}$ at $B=0$ have different enhancement factors because excitons with

different dipole moments interest differently with the x-y plasmon mode of the MNP.[26] For the same reason, the FRET rates for the two excitons become also different. In a high magnetic field, the unusual selection rules for the emission of excitons [curve for 2 T in Fig. 7(d)] originate from the modification of photonic fields in the presence of a plasmonic MNP.

V. CONCLUSIONS

Here we have considered a few examples of hybrid exciton-plasmon systems comprising self-assembled semiconductor quantum dots and metal nanocrystals. For the metals, we took gold and indium and, for semiconductors, we used GaAs and InAs. Spins and plasmons strongly interact in these hybrid systems. This interaction comes from the joint action of the dynamic Coulomb coupling and the spin-dependent exchange interaction. To tune the spin states of excitons in a SQD, we involved a strong magnetic field. In the absorption spectra, the exciton-plasmon interaction leads to several features: asymmetric line shapes (Fano effect), plasmon-induced Lamb shifts of exciton energy, and forbidden optical lines. The forbidden optical lines appear often in the form of antiresonances. Since the exciton-plasmon interaction shifts exciton energies, one can change a spin splitting of exciton by varying the SQD-MNP distance. In the PL spectra, we found theoretically an interesting plasmon-induced modification of optical selection rules in a strong magnetic field.

ACKNOWLEDGMENTS

This work was supported by NSF and Volkswagen Foundation.

APPENDIX A: SPIN-DEPENDENT WAVE FUNCTIONS OF EXCITONS

The spin states of excitons in the presence of a magnetic field are described by the following Hamiltonian:[4]

$$\hat{H}_{spin} = a_z(\hat{J}_{h,z}\cdot\hat{s}_{e,z}) + \sum_{i=x,y,z} b_i(\hat{J}^3_{h,i}\cdot\hat{s}_{e,i}) + \mu_B\left(g_e\hat{s}_{e,z} - \frac{g_h}{3}\hat{J}_{h,z}\right)B,$$

here $\hat{J}_{h,i}$ are the operators of angular momentum of heavy holes and $\hat{s}_{e,i}$ are the electron spin operators. Since we consider only heavy holes, $\hat{J}_{h,i}$ are 2×2 matrices; a_z are b_i are the exchange interaction constants and $g_{e(h)}$ are the g factors. The bright exciton states ($|2\rangle$ and $|3\rangle$) can be written as

$$|j\rangle = F_j|m_z=+1\rangle + G_j|m_z=-1\rangle,$$

where $j=2,3$ and $|m_z=+1\rangle=|s_z=-1/2;\ J_z=+3/2\rangle$ and $|m_z=-1\rangle=|s_z=+1/2;\ J_z=-3/2\rangle$ are the bright states and m_z is the total angular momentum of exciton. Then, the Hamiltonian yields the eigenenergies and eigenstates for the two spin states,

$$\delta E_{spin,12(13)}(B) = \frac{1}{2}(H_2+H_3 \pm \sqrt{(H_2-H_3)^2+4V^2}),$$

$$H_2 = -\frac{3a_z}{4} - \frac{27b_z}{16} - \frac{\Delta E_Z}{2}, \quad H_3 = -\frac{3a_z}{4} - \frac{27b_z}{16} + \frac{\Delta E_Z}{2},$$

$$V = \frac{3(b_x-b_y)}{8},$$

where $\Delta E_Z=\mu_B(g_e+g_h)B$ is the Zeeman splitting. The splitting of the spin states at $B=0$,

$$\Delta_0 = \frac{3}{4}|b_x-b_y|.$$

Then, the amplitudes are derived as

$$F_{2(3)}(B) = \frac{|V|}{\sqrt{V^2+(H_2-\delta E_{spin,12(13)})^2}},$$

$$G_{2(3)}(B) = \frac{|V|(\delta E_{spin,12(13)}-H_2)}{V\sqrt{V^2+(H_2-\delta E_{spin,12(13)})^2}}.$$

Using the Bloch functions for the electrons and heavy holes, we calculate the amplitudes of the absorption process,

$$\langle m_z=+1|\mathbf{r}|gs\rangle = \frac{r_{cv}}{\sqrt{2}}\begin{pmatrix}1\\-i\\0\end{pmatrix}, \quad \langle m_z=-1|\mathbf{r}|gs\rangle = \frac{r_{cv}}{\sqrt{2}}\begin{pmatrix}1\\i\\0\end{pmatrix},$$

where $|gs\rangle=|1\rangle$ is the ground state of the crystal. Important interband matrix elements are now written as

$$\langle j|\mathbf{r}|1\rangle = \frac{r_{cv}}{\sqrt{2}}\left[\begin{pmatrix}1\\-i\\0\end{pmatrix}F_j^* + \begin{pmatrix}1\\i\\0\end{pmatrix}G_j^*\right], \quad j=2,3.$$

The matrix elements for the emission process: $\langle 1|\mathbf{r}|j\rangle = \langle j|\mathbf{r}|1\rangle^*$.

APPENDIX B: A POLARIZABILITY AND FIELDS OF METAL ELLIPSOID

In the general case, the quasistatic matrices for elliptical nanocrystals have the forms

$$\hat{\boldsymbol{\beta}} = \begin{pmatrix}\beta_{xx}&\beta_{xy}&\beta_{xz}\\ \beta_{yx}&\beta_{yy}&\beta_{yz}\\ \beta_{zx}&\beta_{zy}&\beta_{zz}\end{pmatrix}, \quad \hat{\boldsymbol{\gamma}} = \begin{pmatrix}\gamma_{xx}&\gamma_{xy}&\gamma_{xz}\\ \gamma_{yx}&\gamma_{yy}&\gamma_{yz}\\ \gamma_{zx}&\gamma_{zy}&\gamma_{zz}\end{pmatrix}.$$

When the principle axes of an ellipsoid coincide with the coordinate system, these matrices are diagonal and their

components are given by[50]

$$\beta_{ii} = \frac{R_{\mathrm{MNP}x}R_{\mathrm{MNP}y}R_{\mathrm{MNP}z}}{3}\frac{\varepsilon_m - \varepsilon_0}{(\varepsilon_m - \varepsilon_0)L_i + \varepsilon_0},$$

$$\gamma_{ii} = \frac{\varepsilon_0}{(\varepsilon_m - \varepsilon_0)L_i + \varepsilon_0},$$

where $i=x,y,z$ and $R_{\mathrm{MNP}i}$ is the radius of ellipsoid along the i axis.

For a nanorod [Fig. 6(a)], $R_{\mathrm{MNP}x} > R_{\mathrm{MNP}y}=R_{\mathrm{MNP}z}$ and the L parameters are

$$L_x = \frac{1-e^2}{2e^3}\left(Ln\frac{1+e}{1-e} - 2e\right), \quad L_y = L_z = \frac{1}{2}(1-L_x),$$

$$e = \sqrt{1-\left(\frac{R_{\mathrm{MNP}z}}{R_{\mathrm{MNP}x}}\right)^2}.$$

For an oblate ellipsoid [Fig. 7(a)], $R_{\mathrm{MNP}x}=R_{\mathrm{MNP}y} > R_{\mathrm{MNP}z}$ and the L parameters are the following:

$$L_z = \frac{1+e^2}{e^3}(e - \arctan[e]), \quad L_x = L_y = \frac{1}{2}(1-L_z),$$

$$e = \sqrt{\left(\frac{R_{\mathrm{MNP}x}}{R_{\mathrm{MNP}z}}\right)^2 - 1}.$$

*Corresponding author; govorov@ohiou.edu

[1] M. I. D'yakonov and V. I. Perel', Zh. Eksp. Teor. Fiz. **60**, 1954 (1971) [Sov. Phys. JETP **33**, 1053 (1971)].

[2] E. L. Ivchenko and G. E. Pikus, *Superlattices and Other Heterostructures. Symmetry and Optical Phenomena* (Springer, Berlin, 1997).

[3] D. Gammon, E. S. Snow, B. V. Shanabrook, D. S. Katzer, and D. Park, Phys. Rev. Lett. **76**, 3005 (1996).

[4] M. Bayer, A. Kuther, A. Forchel, A. Gorbunov, V. B. Timofeev, F. Schafer, J. P. Reithmaier, T. L. Reinecke, and S. N. Walck, Phys. Rev. Lett. **82**, 1748 (1999).

[5] V. D. Kulakovskii, G. Bacher, R. Weigand, T. Kümmell, A. Forchel, E. Borovitskaya, K. Leonardi, and D. Hommel, Phys. Rev. Lett. **82**, 1780 (1999).

[6] J. G. Tischler, A. S. Bracker, D. Gammon, and D. Park, Phys. Rev. B **66**, 081310 (2002).

[7] A. Högele, S. Seidl, M. Kroner, K. Karrai, R. J. Warburton, B. D. Gerardot, and P. M. Petroff, Phys. Rev. Lett. **93**, 217401 (2004).

[8] J. Berezovsky, O. Gywat, F. Meier, D. Battaglia, X. Peng, and D. D. Awschalom, Nat. Phys. **2**, 831 (2006).

[9] H. Htoon, S. A. Crooker, M. Furis, and S. Jeong, Al. L. Efros, and V. I. Klimov, Phys. Rev. Lett. **102**, 017402 (2009).

[10] D. E. Reiter, T. Kuhn, and V. M. Axt, Phys. Rev. Lett. **102**, 177403 (2009).

[11] C. D. Geddes and J. R. Lakowicz, J. Fluoresc. **12**, 121 (2002).

[12] H. T. Dung, L. Knoll, and D.-G. Welsch, Phys. Rev. A **62**, 053804 (2000).

[13] W. Zhang, A. O. Govorov, and G. W. Bryant, Phys. Rev. Lett. **97**, 146804 (2006).

[14] N. T. Fofang, T. H. Park, O. Neumann, N. A. Mirin, P. Nordlander, and N. J. Halas, Nano Lett. **8**, 3481 (2008).

[15] K. Lopata and D. Neuhauser, J. Chem. Phys. **131**, 014701 (2009).

[16] I. V. Bondarev, L. M. Woods, and K. Tatur, Phys. Rev. B **80**, 085407 (2009).

[17] S. M. Sadeghi, Nanotechnology **20**, 225401 (2009).

[18] M.-T. Cheng, S.-D. Liu, and Q.-Q. Wang, Appl. Phys. Lett. **92**, 162107 (2008).

[19] V. I. Sugakov and G. V. Vertsimakha, Phys. Rev. B **81**, 235308 (2010).

[20] J. Gersten and A. Nitzan, J. Chem. Phys. **75**, 1139 (1981).

[21] E. Dulkeith, M. Ringler, T. A. Klar, J. Feldmann, A. Muñoz Javier, and W. J. Parak, Nano Lett. **5**, 585 (2005).

[22] P. Vasa, R. Pomraenke, S. Schwieger, Yu. I. Mazur, Vas. Kunets, P. Srinivasan, E. Johnson, J. E. Kihm, D. S. Kim, E. Runge, G. Salamo, and C. Lienau, Phys. Rev. Lett. **101**, 116801 (2008).

[23] A. J. Huber, A. Ziegler, T. Koeck, and R. Hillenbrand, Nat. Nanotechnol. **4**, 153 (2009).

[24] A. Urbańczyk, G. J. Hamhuis, and R. Nötzel, Appl. Phys. Lett. **96**, 113101 (2010).

[25] J. Lee, A. O. Govorov, J. Dulka, and N. A. Kotov, Nano Lett. **4**, 2323 (2004).

[26] A. O. Govorov, G. W. Bryant, W. Zhang, T. Skeini, J. Lee, N. A. Kotov, J. M. Slocik, and R. R. Naik, Nano Lett. **6**, 984 (2006).

[27] K. L. Knappenberger, A. M. Schwartzberg, A. M. Dowgiallo, and C. A. Lowman, J. Am. Chem. Soc. **131**, 13892 (2009).

[28] M. Liu, T.-W. Lee, S. K. Gray, P. Guyot-Sionnest, and M. Pelton, Phys. Rev. Lett. **102**, 107401 (2009).

[29] X.-W. Wu, M. Gong, C.-H. Dong, J.-M. Cui, Y. Yang, F.-W. Sun, Z.-F. Han, and G.-C. Guo, Opt. Express **18**, 6340 (2010).

[30] M. M. Maye, O. Gang, and M. Cotlet, Chem. Commun. (Cambridge) **46**, 6111 (2010)..

[31] I. Gerhardt, G. Wrigge, P. Bushev, G. Zumofen, M. Agio, R. Pfab, and V. Sandoghdar, Phys. Rev. Lett. **98**, 033601 (2007).

[32] A. O. Govorov and I. Carmeli, Nano Lett. **7**, 620 (2007).

[33] J. T. Zhang, Y. Tang, K. Lee, and M. Ouyang, Nature (London) **466**, 91 (2010).

[34] A. O. Govorov, Phys. Rev. B **68**, 075315 (2003).

[35] A. O. Govorov, Phys. Rev. B **71**, 155323 (2005).

[36] C. Deneke, W. Sigle, U. Eigenthaler, P. A. van Aken, G. Schuetz, and O. G. Schmidt, Appl. Phys. Lett. **90**, 263107 (2007).

[37] Yu. I. Mazur, W. Q. Ma, X. Wang, Z. M. Wang, G. J. Salamo, M. Xiao, T. D. Mishima, and M. B. Johnson, Appl. Phys. Lett. **83**, 987 (2003); J. H. Lee, Z. M. Wang, K. Sablon, and G. J. Salamo, Cryst. Growth Des. **8**, 690 (2008).

[38] T. V. Shubina, Phys. Status Solidi A **207**, 1054 (2010); T. V. Shubina, A. A. Toropov, V. N. Jmerik, D. I. Kuritsyn, L. V. Gavrilenko, Z. F. Krasil'nik, T. Araki, Y. Nanishi, B. Gil, A. O.

Govorov, and S. V. Ivanov, Phys. Rev. B **82**, 073304 (2010).
[39] V. V. Chaldyshev, J. Appl. Phys. **97**, 024309 (2005).
[40] M. Pfeiffer, K. Lindfors, Ch. Wolpert, P. Atkinson, M. Benyoucef, A. Rastelli, O. G. Schmidt, H. Giessen, and M. Lippitz, arXiv:1007.3646 (unpublished).
[41] U. Woggon, E. Herz, O. Schöps, M. V. Artemyev, Ch. Arens, N. Rousseau, D. Schikora, K. Lischka, D. Litvinov, and D. Gerthsen, Nano Lett. **5**, 483 (2005).
[42] R. Pomraenke, C. Lienau, Y. I. Mazur, Z. M. Wang, B. Liang, G. G. Tarasov, and G. J. Salamo, Phys. Rev. B **77**, 075314 (2008).
[43] J. M. Ulloa, R. Gargallo-Caballero, M. Bozkurt, M. del Moral, A. Guzmán, P. M. Koenraad, and A. Hierro, Phys. Rev. B **81**, 165305 (2010).
[44] In this case, the electric field induced by the incident light is uniform within a SQD and only dipole transitions should be active. Therefore, the oscillator strength of dark states will remain small and the dark states can be neglected.
[45] J. M. Smith, P. A. Dalgarno, R. J. Warburton, A. O. Govorov, K. Karrai, B. D. Gerardot, and P. M. Petroff, Phys. Rev. Lett. **94**, 197402 (2005).
[46] E. D. Palik, *Handbook of Optical Constants of Solids* (Academic Press, New York, 1985).
[47] A. Yariv, *Quantum Electronics*, 2nd ed. (Wiley, New York, 1975).
[48] J.-Y. Yan, W. Zhang, S. Duan, X.-G. Zhao, and A. O. Govorov, Phys. Rev. B **77**, 165301 (2008).
[49] R. Loudon, *The Quantum Theory of Light* (Clarendon, Oxford, 2000).
[50] L. D. Landau and E. M. Lifshitz, *Electrodynamics of Continuous Media* (Pergamon, New York, 1960).